International Journal of
Molecular Sciences

MDPI

Article

Δ^8-THC Protects against Amyloid Beta Toxicity Modulating ER Stress In Vitro: A Transcriptomic Analysis

Agnese Gugliandolo [1], Santino Blando [1], Stefano Salamone [2,3], Diego Caprioglio [2,3], Federica Pollastro [2,3], Emanuela Mazzon [1,*] and Luigi Chiricosta [1]

[1] IRCCS Centro Neurolesi "Bonino-Pulejo", Via Provinciale Palermo, Contrada Casazza, 98124 Messina, Italy
[2] Department of Pharmaceutical Sciences, University of Eastern Piedmont, Largo Donegani 2, 28100 Novara, Italy
[3] PlantaChem Srls, Via Amico Canobio 4/6, 28100 Novara, Italy
* Correspondence: emanuela.mazzon@irccsme.it

Abstract: Alzheimer's disease (AD) represents the most common form of dementia, characterized by amyloid β (Aβ) plaques and neurofibrillary tangles (NFTs). It is characterized by neuroinflammation, the accumulation of misfolded protein, ER stress and neuronal apoptosis. It is of main importance to find new therapeutic strategies because AD prevalence is increasing worldwide. Cannabinoids are arising as promising neuroprotective phytocompounds. In this study, we evaluated the neuroprotective potential of Δ^8-THC pretreatment in an in vitro model of AD through transcriptomic analysis. We found that Δ^8-THC pretreatment restored the loss of cell viability in retinoic acid-differentiated neuroblastoma SH-SY5Y cells treated with $A\beta_{1\text{-}42}$. Moreover, the transcriptomic analysis provided evidence that the enriched biological processes of gene ontology were related to ER functions and proteostasis. In particular, $A\beta_{1\text{-}42}$ upregulated genes involved in ER stress and unfolded protein response, leading to apoptosis as demonstrated by the increase in Bax and the decrease in Bcl-2 both at gene and protein expression levels. Moreover, genes involved in protein folding and degradation were also deregulated. On the contrary, Δ^8-THC pretreatment reduced ER stress and, as a consequence, neuronal apoptosis. Then, the results demonstrated that Δ^8-THC might represent a new neuroprotective agent in AD.

Keywords: Alzheimer's disease; Δ^8-THC; unfolded protein response; neuronal apoptosis

check for updates

Citation: Gugliandolo, A.; Blando, S.; Salamone, S.; Caprioglio, D.; Pollastro, F.; Mazzon, E.; Chiricosta, L. Δ^8-THC Protects against Amyloid Beta Toxicity Modulating ER Stress In Vitro: A Transcriptomic Analysis. *Int. J. Mol. Sci.* **2023**, *24*, 6598. https://doi.org/10.3390/ijms24076598

Academic Editor: Alberto Pérez-Mediavilla

Received: 17 February 2023
Revised: 13 March 2023
Accepted: 31 March 2023
Published: 2 April 2023

Copyright: © 2023 by the authors. Licensee MDPI, Basel, Switzerland. This article is an open access article distributed under the terms and conditions of the Creative Commons Attribution (CC BY) license (https://creativecommons.org/licenses/by/4.0/).

1. Introduction

Alzheimer's disease (AD) is the most common neurodegenerative disorder and represents the most frequent cause of dementia, affecting more than 50 million people worldwide [1,2]. Considering that the strongest risk factor for AD is aging and that life expectancy is gradually increasing, the number of AD patients is also progressively rising [3,4].

Even though AD is mainly sporadic and shows a late onset (>65 years of age), there are rare cases in which the disease is associated with autosomal dominant inheritance and usually develops earlier (between 24 and 60 years of age) [5]. More than 300 pathogenic mutations in presenilin 1 (PSEN1), presenilin 2 (PSEN2), and amyloid precursor protein (APP) genes have been identified in familial AD cases [5]. Instead, allelic variation in the apolipoprotein E (APOE) gene represents a major genetic risk factor for sporadic AD [6].

The most important neuropathological features of AD are β-amyloid (Aβ)-containing extracellular plaques and tau-containing intracellular neurofibrillary tangles [7,8]. In addition, AD is characterized by the atrophy of the cerebral cortex and by the loss of basal forebrain cholinergic neurons [9].

It is known that AD patients generally manifest prominent amnestic cognitive impairment; however, non-amnestic cognitive impairment is less frequent [8]. AD symptoms can vary depending on the stage of the disease and AD can be classified as preclinical

or presymptomatic, mild, and dementia-stage on the basis of the degree of cognitive impairment [4].

Currently, the diagnostic methods for AD primarily rely on neurocognitive tests, brain imaging techniques and cerebrospinal fluid assays [10].

The "amyloid cascade hypothesis" is one of the most important models for the pathogenesis of AD and suggests that the deposition and accumulation of Aβ cause the formation of amyloid plaques, leading to neuronal and synaptic toxicity in the brain. The resulting neuronal damage can lead to memory and cognition dysfunctions [11]. Although the mechanisms implicated in Aβ-induced neurotoxicity are still not completely clarified, it has been suggested that different pathways, including oxidative stress, microglial activation and apoptosis, can be involved [12]. In addition, interestingly, it has been shown that endoplasmic reticulum (ER) stress can be implicated in AD [12]. In particular, it is known that ER is responsible for the biosynthesis of proteins, including the post-translational modification, folding and assembly of newly synthesized proteins, and it has been suggested that the accumulation of insoluble Aβ-peptides could alter ER homeostasis, leading to ER stress and thus activating the unfolded protein response (UPR) [12,13]. Although, at first, UPR aims to restore the normal function of ER, prolonged stress can lead to the activation of apoptotic factors [12]. Considering that it has been shown that ER stress can be involved in Aβ-induced apoptosis, it should be noted that the inhibition of ER stress could exert beneficial effects [12].

Currently, there are no efficacious treatments that are able to reverse or delay the progression of AD [14]. The drugs approved by the US Food and Drug Administration (FDA) for the treatment of AD include the cholinesterase inhibitors donepezil, galantamine and rivastigmine; the N-methyl-D-aspartate (NMDA) receptor antagonist memantine; a combination of memantine and donepezil; the monoclonal antibodies targeting Aβ aducanumab and lecanemab [14–18].

Of note, the possible therapeutic use of cannabinoids in AD has been recently investigated [19]. Studies in rodent models with AD have highlighted the promising effects of cannabinoids in decreasing amyloid plaque deposition and inducing hippocampal neurogenesis, whereas clinical studies have shown the beneficial effects of cannabinoid treatment on AD symptoms [20].

In particular, it has been suggested that delta8-tetrahydrocannabinol (Δ^8-THC), a cannabinoid that is a structural isomer of a widely known active ingredient in cannabis delta9-tetrahydrocannabinol (Δ^9-THC), could exert interesting pharmacological effects [21,22]. It is considered to have fewer potent psychoactive properties than Δ^9-THC [23]. Δ^8-THC is a partial agonist of the cannabinoid CB1 receptor, while it has also been reported to be an agonist or inverse agonist at the CB2 receptor. Cannabinoids can also interact with other receptors, such as PPARγ and GRP55, but there are no data about Δ^8-THC effects on these receptors [22]. Δ^8-THC use may be associated with decreased chemotherapy side effects, analgesic effects, decreased seizure activity, lower intra-ocular eye pressure, decreased cancer cell proliferation, decreased depressive symptoms and decreased nicotine use and withdrawal [23]. In addition, it has been shown that Δ^8-THC exerts moderate inhibitory activity against acetylcholinesterase and butyrylcholinesterase [24]. This is of particular interest, considering that it is known that the enhancement of cholinergic neurotransmission through cholinesterase inhibitors is the leading therapeutic option for treating the cognitive and behavioral symptoms of the early and late stages of AD [25].

In this study, we evaluated the neuroprotective potential of Δ^8-THC in an in vitro model of AD using Next Generation Sequencing (NGS). With this aim, we pretreated retinoic acid (RA)-differentiated SH-SY5Y neuroblastoma cells with Δ^8-THC and exposed them to $A\beta_{1\text{-}42}$. At the end of the treatment, we performed a transcriptomic analysis in order to evaluate whether Δ^8-THC could modulate signaling pathways leading to protective effects.

2. Results

2.1. Δ^8-THC Counteracted the Aβ_{1-42}-Induced Loss of Cell Viability

RA-differentiated SH-SY5Y were pretreated with different doses of Δ^8-THC for 24 h and, after, were treated with 10 μM Aβ_{1-42} for another 24 h. Using the MTT assay, we evaluated if Δ^8-THC exerted toxicity in the range of the doses tested (5–20 μM) and if it was able to counteract Aβ_{1-42} toxicity.

The MTT assay results demonstrated that 10 μM Aβ_{1-42} treatment reduced the cell viability of RA-differentiated SH-SY5Y cells. Δ^8-THC was not cytotoxic at all the concentrations tested. However, 5 μM Δ^8-THC was not able to counteract Aβ_{1-42}-reduced cell viability. On the contrary, both 10 and 20 μM Δ^8-THC were able to restore the cell viability of RA-differentiated SH-SY5Y cells after 10 μM Aβ_{1-42} treatment (Figure 1). Transcriptomic analysis was carried out using the concentration 20 μM Δ^8-THC.

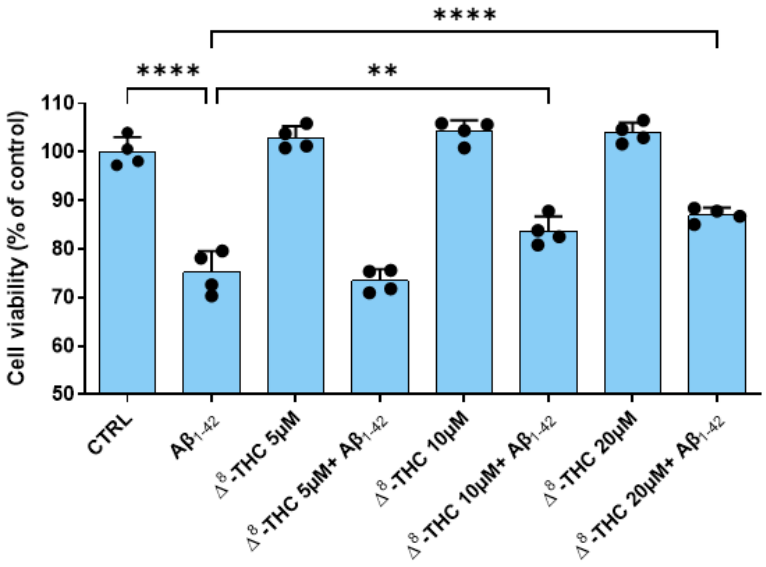

Figure 1. Cell viability after Aβ_{1-42} and Δ^8-THC treatment. The treatment with 10 μM Aβ_{1-42} reduced cell viability of RA-differentiated SH-SY5Y cells, but Δ^8-THC pretreatment at the concentrations 10 and 20 μM was able to restore cell viability. N = 4 independent experiments. The results are expressed by mean ± standard deviation (SD). ** $p < 0.01$; **** $p < 0.0001$.

2.2. Transcriptomic Analysis Revealed That Δ^8-THC Counteracted the Aβ_{1-42}-Induced ER Stress

In order to evaluate the differential pattern of gene expression in RA-differentiated SH-SY5Y treated with 20 μM Δ^8-THC and 10 μM Aβ_{1-42}, we performed NGS transcriptomic analysis. The aim was to evaluate the pathways associated with the protective effects exerted by Δ^8-THC. Figure 2 represents the distribution of differentially expressed genes (DEGs) between control against Aβ_{1-42} (CTRL vs. Aβ_{1-42}), control against Δ^8-THC (CTRL vs. Δ^8-THC), or Aβ_{1-42} against Δ^8-THC + Aβ_{1-42} groups (Aβ_{1-42} vs. Δ^8-THC + Aβ_{1-42}). In the blue section, we highlighted how many DEGs were exclusively deregulated in each comparison (1896 in CTRL vs. Aβ_{1-42}, 1812 in CTRL vs. Δ^8-THC and 2597 in Aβ_{1-42} vs. Δ^8-THC + Aβ_{1-42}), between two comparisons and not in the last one (2323 not in Aβ_{1-42} vs. Δ^8-THC + Aβ_{1-42}, 752 not in CTRL vs. Aβ_{1-42}, 1479 not in CTRL vs. Δ^8-THC) or deregulated in all the comparisons (1366 DEGs). On the other hand, the three donuts show how many upregulated (dark red) or downregulated (light red) DEGs were found between each comparison and, in particular, between CTRL vs. Aβ_{1-42} and CTRL vs. Δ^8-THC in the left-top section, CTRL vs. Aβ_{1-42} and Aβ_{1-42} vs. Δ^8-THC + Aβ_{1-42} in the bottom section and CTRL vs. Δ^8-THC and Aβ_{1-42} vs. Δ^8-THC + Aβ_{1-42} in the right-top section.

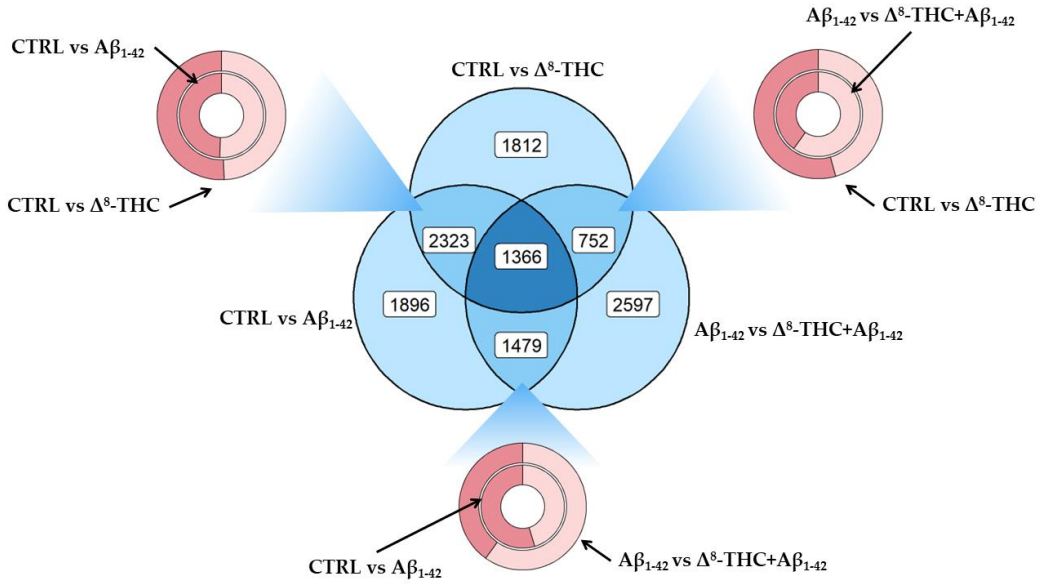

Figure 2. DEGs distribution between CTRL vs. $A\beta_{1\text{-}42,}$ CTRL vs. Δ^8-THC groups or $A\beta_{1\text{-}42}$ vs. Δ^8-THC + $A\beta_{1\text{-}42}$. Venn diagram in the center of the plot highlights the amount of DEGs found exclusively in each comparison (outer circles), how many DEGs found in two groups but not in the other (intersection of two circles) or how many DEGs were found in each comparison (center of the diagram). Each donut plot highlights, in turn, the intersection of two comparisons showing in dark red the upregulated and in the light red the downregulated DEGs.

We then enriched DEGs both in CTRL vs. $A\beta_{1\text{-}42}$ and $A\beta_{1\text{-}42}$ vs. Δ^8-THC + $A\beta_{1\text{-}42}$ in order to evaluate if Δ^8-THC was able to exert protective effects through the modulation of processes affected by $A\beta_{1\text{-}42}$. Specifically, we enriched DEGs for the biological process terms of gene ontology (GO) that revealed 665 terms in CTRL vs. $A\beta_{1\text{-}42}$ and 488 terms in $A\beta_{1\text{-}42}$ vs. Δ^8-THC + $A\beta_{1\text{-}42}$ groups. The inspection of the biological process terms commonly enriched in the two analyses revealed 321 terms. In this line, we depicted the bubble plot in Figure 3 that shows how DEGs were enriched for each ontology in the CTRL vs. $A\beta_{1\text{-}42}$ (orange) or $A\beta_{1\text{-}42}$ vs. Δ^8-THC + $A\beta_{1\text{-}42}$ (light blue) groups. They demonstrated the "regulation of ubiquitin-dependent protein catabolic process" (GO:2000058), "neuron death" (GO:0070997), the "regulation of proteasomal protein catabolic process" (GO:0061136), "neuron apoptotic process" (GO:0051402), "positive regulation of protein catabolic process" (GO:0045732), "proteasome-mediated ubiquitin-dependent protein catabolic process" (GO:0043161), "regulation of protein catabolic process" (GO:0042176), "regulation of protein ubiquitination" (GO:0031396), "proteasomal protein catabolic process" (GO:0010498), "protein polyubiquitination" (GO:0000209). Interestingly, all the aforementioned ontologies included a higher number of DEGs in CTRL vs. $A\beta_{1\text{-}42}$ than in $A\beta_{1\text{-}42}$ vs. Δ^8-THC + $A\beta_{1\text{-}42}$ groups.

Given that significantly enriched GO are related to ER functions and proteostasis, we focused on related DEGs looking at KEGG pathways "Alzheimer disease" (hsa05010) and "protein processing in endoplasmic reticulum" (hsa04141). In Table 1, we report the common DEGs, altered in both CTRL vs. $A\beta_{1\text{-}42}$ and $A\beta_{1\text{-}42}$ vs. Δ^8-THC + $A\beta_{1\text{-}42}$. In the supplementary Table S1, we report all the inspected DEGs.

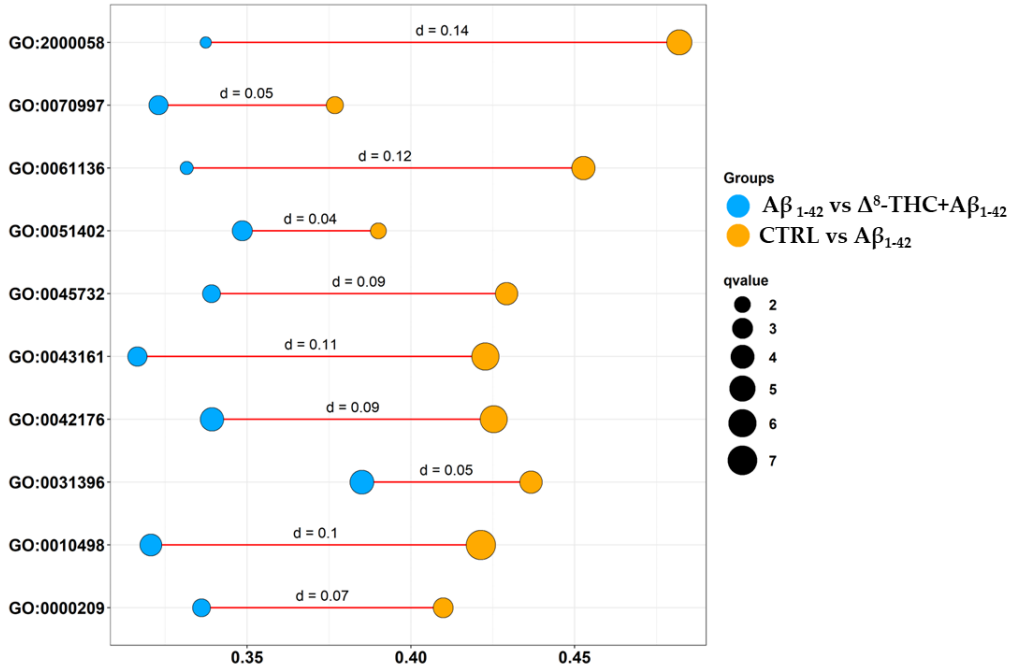

Figure 3. Bubbleplot of biological process terms enriched in gene ontology between CTRL vs. $A\beta_{1\text{-}42}$ and $A\beta_{1\text{-}42}$ vs. Δ^8-THC + $A\beta_{1\text{-}42}$ groups. For each ontology reported on the *y* axis, a bubble for the CTRL vs. $A\beta_{1\text{-}42}$ (orange) and one for the $A\beta_{1\text{-}42}$ vs. Δ^8-THC + $A\beta_{1\text{-}42}$ (light blue) groups were plotted. The position of the bubble in the *x* axis shows the number of DEGs in the ontology (the more on the right, the higher the number of DEGs). The number of DEGs was normalized over the number of genes included in the ontology term itself so that the terms were comparable to each other. The size of the bubble is a score given by −log(q-value).

Table 1. Common DEGs, altered in both CTRL vs. $A\beta_{1\text{-}42}$ and $A\beta_{1\text{-}42}$ vs. Δ^8-THC + $A\beta_{1\text{-}42}$, related to "Alzheimer's disease" (hsa05010) and "protein processing in endoplasmic reticulum" (hsa04141) pathways.

Gene	CTRL vs. $A\beta_{1\text{-}42}$		$A\beta_{1\text{-}42}$ vs. Δ^8-THC + $A\beta_{1\text{-}42}$		CTRL vs. Δ^8-THC	
	Fold Change	**q-Value**	**Fold Change**	**q-Value**	**Fold Change**	**q-Value**
ATF6	0.11	9.70×10^{-7}	−0.11	9.51×10^{-08}		
BCL2	−0.45	1.74×10^{-17}	0.33	1.08×10^{-10}	−0.34	3.16×10^{-11}
DNAJA2	−0.11	8.15×10^{-4}	0.10	1.40×10^{-03}		
DNAJC1	0.21	1.51×10^{-3}	−0.25	3.70×10^{-05}		
EDEM1	−0.29	3.16×10^{-9}	0.17	4.10×10^{-04}		
EIF2AK4	0.15	1.51×10^{-15}	−0.14	4.64×10^{-16}	0.15	8.77×10^{-15}
ERN1	0.37	1.46×10^{-6}	−0.19	7.29×10^{-03}		
FBXO6	−1.21	2.21×10^{-4}	1.52	3.86×10^{-07}		
HSP90AA1	0.06	3.31×10^{-33}	0.01	5.68×10^{-03}	0.11	3.57×10^{-129}
HSP90AB1	0.04	2.31×10^{-25}	−0.02	6.86×10^{-05}	0.10	1.97×10^{-145}
HSP90B1	0.06	2.20×10^{-12}	−0.02	1.15×10^{-03}	0.10	6.80×10^{-43}
MAN1B1	0.10	1.70×10^{-8}	−0.08	3.89×10^{-06}		
OS9	0.16	2.08×10^{-17}	−0.12	3.05×10^{-12}		
PSMB4	−0.09	5.43×10^{-13}	−0.06	4.45×10^{-06}		
PSMB5	−0.18	3.86×10^{-14}	0.14	2.98×10^{-09}	0.09	2.45×10^{-4}
PSMB6	0.14	1.82×10^{-3}	0.15	7.90×10^{-05}	0.21	1.16×10^{-6}
RAD23A	−0.15	2.61×10^{-6}	0.09	4.40×10^{-03}		
SEC61B	0.12	1.06×10^{-3}	−0.23	7.89×10^{-13}		
TXNDC5	−4.20	2.95×10^{-4}	3.22	8.52×10^{-03}		
UBE2G2	−0.11	2.31×10^{-3}	0.13	5.66×10^{-05}		
UBE2J1	−0.11	7.60×10^{-5}	0.11	6.06×10^{-06}		
UBXN6	−0.11	4.66×10^{-5}	0.11	1.41×10^{-05}	0.08	2.60×10^{-3}
UBXN8	−0.26	1.57×10^{-5}	0.15	8.50×10^{-03}		

The column fold change shows for each DEG the difference in the level of expression computed by $\log_2(A\beta_{1\text{-}42}/\text{CTRL})$, $\log_2(\Delta^8\text{-THC} + A\beta_{1\text{-}42}/A\beta_{1\text{-}42})$ or $\log_2(\Delta^8\text{-THC/CTRL})$. The *q*-Value column was obtained correcting the *p*-value through Benjamini–Hochberg correction. All values were rounded to the second decimal digit.

2.3. Δ^8-THC Restored the Protein Levels of Bax and Bcl-2

In order to evaluate the effects of Δ^8-THC on A$\beta_{1\text{-}42}$-induced apoptosis, we evaluated the levels of Bax and Bcl-2. Western blot analysis evidenced a significant increase in Bax in RA-differentiated SH-SY5Y treated with 10 µM A$\beta_{1\text{-}42}$. Pre-treatment with 20 µM Δ^8-THC was able to reduce Bax protein levels. On the contrary, Bcl-2 protein levels were decreased in A$\beta_{1\text{-}42}$ treated cells, while Δ^8-THC restored its levels (Figure 4). Δ^8-THC treated RA-differentiated SH-SY5Y showed a level of Bax similar to the control, while Bcl-2 increased.

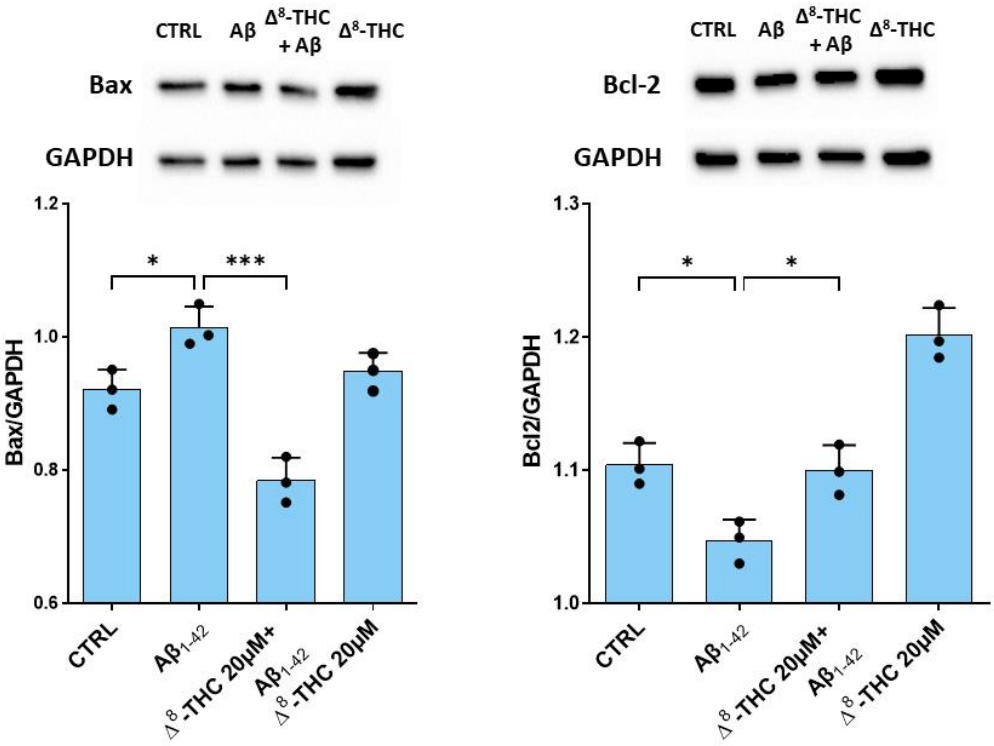

Figure 4. Western blot for Bax and Bcl-2. A$\beta_{1\text{-}42}$ treatment caused an increase in Bax and a reduction in Bcl-2 protein levels. Δ^8-THC treatment restored protein levels of Bax and Bcl-2. N = 3 independent experiments. The results are expressed by mean ± standard deviation (SD). * $p < 0.05$; *** $p < 0.001$.

3. Discussion

The prevalence of dementia is increasing, and it is expected that about 113 million will be affected in 2050 worldwide [26]. Given that AD is the prevalent form of dementia, it is of main importance to find new therapeutic strategies. Cannabinoids seem promising for neuroprotective treatments. Some of them have been reported to improve cognitive functions and reduce Aβ [20]. Δ^8-THC is present in a very low quantity in plants, and it is mainly produced by cannabidiol. Δ^8-THC is a structural isomer of the Δ^9-THC, showing a double bond between carbon atoms 8 and 9 rather than carbon atoms 9 and 10. Δ^9-THC is responsible for the psychoactive properties of cannabis, such as alterations in mood, perception and cognition. Δ^9-THC is one of the cannabinoids most studied, but Δ^8-THC has also been attracting attention for the better thermodynamic stability in comparison to Δ^9-THC. The two compounds showed similar pharmacokinetics and pharmacodynamics. Both Δ^8-THC and Δ^9-THC are partial agonists of the cannabinoid receptor CB1, but Δ^8-THC showed a lower affinity. Given that the psychoactive effects of Δ^9-THC depend on the CB1 receptor, Δ^8-THC has a lower psychotropic potency. Both Δ^8-THC and Δ^9-THC were reported to act as agonists or inverse agonists at the CB2 receptor [22]. A survey of consumers highlighted that Δ^8-THC might exert the benefits of Δ^9-THC with lower risks [27].

Some cannabinoids have already shown protective effects in both in vitro and in vivo AD models. Δ^9-THC was shown to lower Aβ levels in an in vitro AD model in a dose-dependent manner, directly binding to the Aβ peptide and inhibiting its aggregation [28]. Moreover, it can alleviate cognitive impairments and reduce inflammatory markers, the numbers of Aβ plaques and degenerated neurons in AD mice [29–31]. Additionally, other agonists of CB1 and CB2 receptors were tested in AD models. ACEA, a CB1 receptor agonist, exerted a strong neuroprotective action against Aβ toxicity in vitro and in vivo [32,33]. Additionally, CB2 agonists, such as JWH-133, showed neuroprotective effects in AD models, reducing inflammation, Aβ plaque and deposition, increasing Aβ clearance and improving cognitive performance [34]. CP55940, an agonist of CB1 and CB2, restored mitochondrial membrane potential and reactive oxygen species and reduced extracellular Aβ [35].

However, the potential neuroprotective effects of Δ^8-THC have not been investigated yet. To our knowledge, this is the first study that has investigated Δ^8-THC effects in an in vitro model of AD.

In this study, we found that Δ^8-THC showed no cytotoxicity at all the doses tested. Interestingly, it was able at doses 10 and 20 μM to restore the loss of cell viability induced by $A\beta_{1\text{-}42}$. The dose of 20 μM Δ^8-THC was used for other experiments.

Transcriptomic analysis and GO evaluations evidenced the enrichment of biological processes related to proteostasis and neuronal apoptosis. Then, Δ^8-THC could modulate the pathways involved in proteostasis to exert protective effects. For this reason, we focused on DEGs related to ER functions and proteostasis, looking at the KEGG pathways for "Alzheimer's disease" (hsa05010) and "protein processing in endoplasmic reticulum" (hsa04141).

ER plays important roles in protein biosynthesis and in their quality control. In some cases, the maintenance of cellular homeostasis is not possible, causing a reduction in the protein folding capacity of ER and leading to the accumulation of misfolded/unfolded proteins in ER. This process caused the disruption of cellular homeostasis, inducing ER stress. AD is characterized by protein misfolding and aggregation and Aβ accumulation, which are all events that trigger ER stress [36].

Treatment with $A\beta_{1\text{-}42}$ also altered the expression of several chaperones. Chaperones are a functionally related group of proteins that assist protein folding both in physiological and stress conditions. Among chaperones, heat shock proteins (HSPs) are well known. HSPs have a role in all the phases of proteostasis; they participate in folding, protein synthesis and degradation. Their levels increase during stress exposure, helping to prevent conformational changes and the aggregation of misfolded proteins [37]. We found that several HSPs were dysregulated by $A\beta_{1\text{-}42}$ treatment. $A\beta_{1\text{-}42}$ treatment increased the expression of several members of the HSP40 family (*DNAJC1*, *DNAJC10*, *DNAJC3*), HSP70 family (*HSPA1A* and *HSPA1L*) and HSP90 family (*HSP90AA1* and *HSP90AB1*). HSPs also played a role in the degradation of proteins by the proteasome. The genes encoding for these HSPs, such as *DNAJA2* and *DNAJB12*, were downregulated by $A\beta_{1\text{-}42}$ treatment.

We also found the upregulation of *HSP90B1*, encoding for GRP94, after $A\beta_{1\text{-}42}$ treatment. GRP94 is a chaperone that directs the folding and/or assembly of proteins. Moreover, GRP94 is one of the few major luminal calcium-binding proteins. It seems to have a role in ER-associated degradation (ERAD) to distinguish misfolded proteins and target them for degradation [38]. Δ^8-THC reduced the levels of *HSP90B1*, *DNAJC1* and *HSP90AB1* while increasing *DNAJA2* expression in cells treated with $A\beta_{1\text{-}42}$.

The excess of misfolded proteins induces ER stress. In order to counteract ER stress, cells activate UPR. The UPR starts as cell-protective cascades, with the aim of reducing the ER load of unfolded proteins through the inhibition of protein synthesis and the upregulation of protein folding and degradation. However, prolonged UPR finally leads to cell death. The UPR signaling involves three sensor proteins, which are PERK, ATF6, and IRE1. Abnormal levels of these effectors of UPR were reported in AD brains [39]. We found the upregulation of PERK (*EIFAK2* and *EIFAK4*), ATF6 (*ATF6*) and IRE1 (*ERN1*) in cells treated with $A\beta_{1\text{-}42}$. PERK activation is reported in AD and is associated with

neurodegeneration and memory deficits [40]. Additionally, IRE1 activation is known to participate in AD pathogenesis and to be positively correlated with the progression of AD [41]. IRE1 activation is also associated with the induction of apoptosis [42]. Active ATF6 has also been shown in AD models [42]. We also found the downregulation of *WFS1*, which influences ER stress, to negatively regulate ATF6α [43]. Interestingly, it was found that the protein level of WFS1 and the number of WFS1+ neurons decreased in both AD-like mouse model brains and human post-mortem AD [44]. In particular, WFS1 deficiency was linked with increased tau pathology and neurodegeneration. WFS1 deficiency may induce chronic ER stress and affect the degradation and clearance of tau aggregates [45]. Interestingly, Δ^8-THC pre-treatment reduced the expression of the genes encoding for PERK, ATF6 and IRE1.

Misfolded/unfolded proteins are eliminated by the proteasome through ERAD. ERAD can be divided into four steps that are substrate recognition, dislocation across the membrane, ubiquitination and degradation by the proteasome [46]. The data suggest alterations of ERAD in AD [47–50]. In this study, we found a dysregulation of genes involved in the ERAD process. Specifically, genes involved in the phase of the recognition of unfolded protein were upregulated by $A\beta_{1\text{-}42}$. We found the upregulation of genes encoding for ERManI (*MAN1A2* and *MAN1B1*). Removal of mannose residues is a critical process in targeting misfolded glycoproteins for degradation. This removal is operated by ERManI together with EDEM [51,52]. This trimming permits misfolded glycoproteins to be bound to OS-9 and XTP3-B, which target them to ERAD. OS-9 is upregulated in response to ER stress and is required for the ubiquitination of ERAD substrates, suggesting that it may help transfer misfolded proteins to ubiquitination machinery [53]. OS9 and XTP3B redundantly promote glycoprotein degradation, but XTP3B inhibits the degradation of non-glycosylated proteins, while OS9 antagonizes this inhibition [54]. After treatment with $A\beta_{1\text{-}42,}$ we also found the upregulation of OS-9 and XTP3B (*ERLEC1*). We also found the downregulation of *EDEM1*. It can modulate APP metabolism, and its overexpression is associated with a decrease in Aβ secretion [55]. Interestingly, *EDEM1* can be upregulated by Δ^8-THC pre-treatment. Δ^8-THC pre-treatment also reduced OS-9 and *MAN1B1*.

We also found deregulation in the genes encoding for PDI (*PDIA6*, *P4HB*, *TXNDC5*) and ERO (*ERO1A*). $A\beta_{1\text{-}42}$ increased the genes encoding for ERO while reducing the expression of those encoding for PDI. In the oxidizing environment of the ER, unfolded proteins interact with PDI and undergo oxidative protein folding. In this way, misfolded substrate proteins can be reduced and refolded or isomerized to the appropriate native protein conformation. Misfolded proteins are reduced and isomerized by PDI and converted to their appropriate native conformation. Then, reduced PDI is reoxidized by ERO1. Δ^8-THC pre-treatment reduced ERO (*ERO1B*) while also increasing PDI (*ERP29* and *TXNDC5*).

On the contrary, the genes involved in the processes of translocation, ubiquitination and degradation were mainly downregulated by $A\beta_{1\text{-}42}$. Bap31, encoded by *BCAP31* which we found downregulated, have several roles in ER homeostasis: membrane protein chaperone, quality control, and it is involved in ER stress and ERAD [56]. Its deficiency was associated with the formation of Aβ plaques in a murine AD model [57]. P97, encoded by *VCP*, also plays a critical role in protein dislocation in ERAD [46]; it is involved in aggregates clearance, and, indeed, its knockdown delayed the elimination of ubiquitin-positive aggregates [58]. We found the downregulation of *VCP* after $A\beta_{1\text{-}42}$ treatment.

The poly-ubiquitination of proteins is fundamental for their degradation by the proteasome, and different enzymes are required: an E1 activating enzyme activates ubiquitin in an ATP-dependent manner, an E2 ubiquitin-conjugating enzyme (Ubc), and an E3 ubiquitin-protein ligases that mediate the transfer of ubiquitin from the Ubc enzyme onto the target substrate. We found a downregulation in ubiquitin ligase complex subunits after treatment with $A\beta_{1\text{-}42}$, such as *UBE2G2* and others (*RBX1*, *UBE2J1*, *UBQLN1*, *UBQLN2*, *UBQLN4*, *UBXN6*, *UBXN8*). UBE2G2 was shown to be critically important for degradation through the ERAD of multiple substrates [59]. Additionally, *FBXO6* was downregulated; it is a

functional E3 ubiquitin ligase that plays a critical role in inhibiting ER stress-induced apoptosis [60].

Δ^8-THC pretreatment was able to reverse the alterations of the gene expression induced by Aβ_{1-42}. In particular, the genes involved in protein targeting (*EDEM3*, *MAN1B1*) were downregulated, suggesting that there was less need for proteins involved in unfolded protein recognition. *SEC61A1* and *SEC61B* were downregulated. The Sec61, which interacts with TRAP [61], encoded by *SSR3,* which was upregulated, mediates protein import into the ER and is also a candidate channel for the dislocation of ERAD substrates [62,63]. The expression of the genes involved in protein dislocation and ubiquitination increases (*UBE2G2*, *SELENOS*, *TRAM1*, *UBE2J1*, *UBXN6*, *UBXN8*, *FBXO6*). Then, if needed, misfolded/unfolded proteins can be dislocated to the cytosol and ubiquitinated.

Interestingly, Δ^8-THC reduced the expression of *HERPUD1*, encoding for HERP. HERP was reported to be involved in Aβ accumulation, including the formation of senile plaques [64]. Δ^8-THC also increased *DERL1*, encoding for Derlin-1, which plays a main role in the transport to the cytosol [65,66].

Δ^8-THC also increased the expression of the shuttling factor *RAD23A* that delivers ubiquitin conjugates to the proteasome and activates its degradative capacity. Δ^8-THC also restored the expression of other genes that were involved in substrate delivery to the proteasome, such as *ATXN3* [67].

Aβ_{1-42}-treated cells also showed a downregulation of the genes encoding for 20S proteasome (*PSMA5*, *PSMB2*, *PSMB3*, *PSMB4*, *PSMB5*, *PSMB7*). The 20S proteasome was shown to be able to degrade misfolded, oxidized and intrinsically disordered proteins, but also Aβ, and to be the major degradation machinery under oxidizing conditions [68,69]. The 20S proteasome was reported to be inhibited in regions affected by Aβ, and Aβ aggregates were shown to inhibit proteasome activity in vitro [70]. It was shown that the Aβ precursor protein reduced the expression of the proteasome subunit α type-5 and β type-7, leading to cell death [71]. In line with the previous work, also in our work, these subunits were downregulated by Aβ_{1-42} treatment. Δ^8-THC was able to partially upregulate the expression of proteasome subunits (*PSMB5*, *PSMB6*). In particular, we found the upregulation of *PSMB5,* whose overexpression was associated with increased resistance to Aβ_{1-42} toxicity [72].

As we also said before, ER stress can trigger neuronal apoptosis. The Aβ_{1-42}-induction of cell death in our study was demonstrated by the increase in *BAX* and the reduction in *BCL2* gene expression. The transcriptomic results were also supported by Western blot analysis, which showed an increase in Bax protein levels and Bcl-2 reduction. Δ^8-THC pre-treatment reduced apoptosis induced by Aβ_{1-42}, as demonstrated by the increase in Bcl-2 and the reduction in Bax levels.

RA-differentiated SH-SY5Y cells treated only with Δ^8-THC showed no ER stress; indeed, *ATF6* and *ERN1* were not differentially expressed compared to the control cells, and *EIFAK3* was downregulated. Moreover, it increased some of the genes involved in the dislocation of misfolded proteins, such as *DERL1, VCP, SSR3* and some proteasome subunits, including *PSMB5,* suggesting an efficient degradation of potentially unfolded proteins.

Figure 5 reports the proteins encoded by DEGs and modulated in Aβ_{1-42} and Δ^8-THC treated groups in the ER pathway.

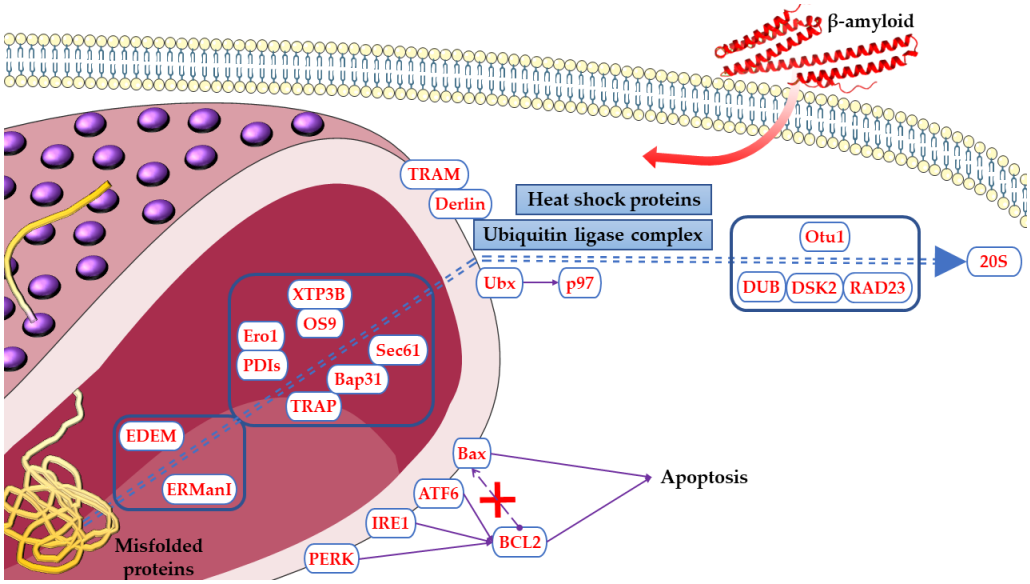

Figure 5. Proteins encoded by DEGs modulated in $A\beta_{1\text{-}42}$ and Δ^8-THC treated cells in ER pathway. The name of the shown proteins was obtained by KEGG. The figure was drawn using the vector image bank of Servier Medical Art by Servier (http://smart.servier.com/, accessed on 10 February 2023). Licensed under a Creative Commons Attribution 3.0 Unported License (https://creativecommons.org/licenses/by/3.0/, accessed on 10 February 2023).

4. Materials and Methods

4.1. Synthesis and Purification of Δ^8-THC

To a stirred solution of CBD (200 mg, 0.636 mmol, 1eq) in DCM (5 mL), *p*-toluensulfonic acid (11 mg, 0.064 mmol, 0.1 eq) was added. The reaction was refluxed for 6 h, followed by TLC (R*f* = 0.67, silica, petroleum ether-EtOAc 95:5) until the complete conversion of the starting material, which was then quenched with $NaHCO_3$ s.s. and diluted with DCM. The combined organic phases were washed with brine, dried, and evaporated. The residue was purified by GCC on silica gel (pure petroleum ether to petroleum ether-EtOAc 9:1) to afford 182 mg (91%) of Δ^8-THC as a brown oil.

This latter impure Δ^8-THC (1) (Figure 6) was purified with JASCO Hichrom, 250 × 25 mm, silica UV−vis detector-2075 plus (silica, petroleum-ether-EtOAc gradient from 95:5 to 85:15) to afford 150 mg of Δ^8-THC (1, 99%) as a brownish powder, whose structure was identified according to ^{1}H NMR (Figure S1) and reported in the literature [73]. ^{1}H 400 MHz NM spectra were measured on Bruker 400 spectrometers (Bruker®, Billerica, MA, USA). Chemical shifts were referenced to the residual solvent signal ($CDCl_3$: δH = 7.26). Silica gel 60 (70-230 mesh) used for low-pressure chromatography was purchased from Macherey-Nagel (Düren, Germany). Purifications were monitored by TLC on Merck 60 F254 (0.25 mm) plates, visualized by staining with 5% H_2SO_4 in EtOH and heating. Chemical reagents and solvents were from Aldrich (Darmstadt, Germany) and were used without any further purification unless stated otherwise. HCPL JASCO Hichrom, 250 × 25 mm, silica UV−vis detector-2075 plus (Tokyo, Japan).

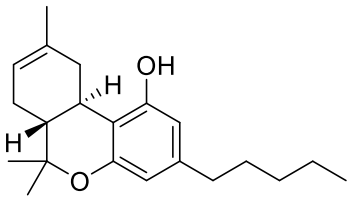

1

Figure 6. Δ^8-THC chemical structure.

4.2. Cell Culture and Differentiation

The human neuroblastoma cell line SH-SY5Y was acquired from American Type Culture Collection (ATCC) (Manassas, VA, USA). Cells were grown in a monolayer at 37 °C in a 5% CO_2 humidified atmosphere using Dulbecco's Modified Eagle's Medium/Nutrient Mixture F-12 Ham (DMEM/F12) medium (Sigma-Aldrich, St. Louis, MO, USA) supplemented with 10% fetal bovine serum (FBS) (Sigma-Aldrich), 1% glutamine, and 1% penicillin-streptomycin (100 U-100 µg/mL). With the aim of inducing neuronal differentiation, SH-SY5Y cells were incubated for 5 days with 10 µM of RA (Sigma-Aldrich).

4.3. Cell Treatment with $A\beta_{1-42}$ and Δ^8-THC

$A\beta_{1-42}$ (Sigma-Aldrich, St. Louis, MO, USA) was dissolved in dimethyl sulfoxide (DMSO), diluted in phosphate-buffered saline (PBS), aggregated at 37 °C for 24 h, and added to the medium at the concentration 10 µM (final DMSO concentration was <0.1%). It has been demonstrated that $A\beta_{1-42}$ incubation for 24 h at 37 °C induced the formation of aggregates [74]. Δ^8-THC was dissolved in DMSO, diluted in PBS and added at the final concentration in the medium (the final DMSO concentration was <0.1%). Cells were pre-treated with Δ^8-THC for 24 h. At the end of the pre-treatment, cells were treated with the medium containing 10 µM of $A\beta_{1-42}$ for 24 h. This concentration of $A\beta_{1-42}$ was chosen based on previous studies showing that it was able to exert cytotoxicity in SH-SY5Y cells [75–84]. Control cells and cells pretreated with Δ^8-THC were incubated with DMEM/F12 medium supplemented with 10% FBS.

4.4. Cell Viability

Cell viability was evaluated with a Thiazolyl Blue Tetrazolium Bromide (MTT) assay. SH-SY5Y cells were cultured in 96-well plates, underwent RA differentiation, and were treated as reported in the previous paragraph. At the end of the treatment, the cells were incubated with a medium containing MTT (0.5 mg/mL; Sigma-Aldrich) at 37 °C for 4 h. The formed formazan crystals were dissolved in acidic isopropanol at 37 °C for 1 h, and the optical density was evaluated by the spectrophotometric measurement of absorbance using the microplate reader Victor NIVO™ (PerkinElmer, Waltham, MA, USA).

4.5. Extraction of Total RNA and cDNA Library Preparation

RNA extraction was carried out with a Maxwell® RSC simplyRNA Cells Kit (Promega, Madison, WI, USA) according to the manufacturer's instruction. The preparation of the library was performed following the TruSeq RNA Exome protocol (Illumina, San Diego, CA, USA) as previously described [75].

4.6. RNA-Seq Data Analysis and Gene Evaluation

The raw data obtained from the NextSeq 550 Dx instrument of Illumina was evaluated using the fastqc tool version 0.11.4 from the Babraham Institute in Cambridge, UK. Adapters and low-quality bases were then eliminated through Trimmomatic [85] version 0.38 (Usadel Lab, Aachen, Germany). The cleaned reads were aligned to the human reference genome (GRCh38) using the STAR RNA-seq aligner [86] 2.7.3a (New York, NY, USA). The expression levels of the transcripts were computed using the htseq-count python package [87] version 0.6.1p1 (European Molecular Biology Laboratory (EMBL), Heidelberg, Germany). DEGs were identified using the DESeq2 library in R [88] version 3.6.3 (R Core Team). No cut-off was set on the fold change. Nevertheless, to drop false positive DEGs, the Benjamini–Hochberg procedure was used with a tight q-value of 0.01. The enrichment of the biological process terms of the gene ontology was also performed in R using the package biomaRt [89] version 2.52.0. Plots were depicted using the R libraries ggplot2 version 3.4.0 and ggVennDiagram version 1.2.2.

4.7. Protein Extraction and Western Blot Analysis

At the end of the treatment, SH-SY5Y were harvested with trypsin-Ethylenediaminetetraacetic acid (EDTA), and proteins were extracted using RIPA (Thermo Scientific™, Waltham, MA, USA) according to the manufacturer's instruction. Protein concentration was evaluated using the Bio-Rad Protein Assay (Bio-Rad Laboratories, Hercules, CA, USA) and bovine serum albumin (BSA) as standard. Twenty-five micrograms of proteins were separated on sodium dodecyl sulfate-polyacrylamide gel electrophoresis (SDS-PAGE) and transferred onto a PVDF transfer membrane (Immobilon-P PVDF, Merck Millipore division of Merck KGaA, Darmstadt, Germany). Membranes were blocked for 1 h at room temperature, with PBS containing 5% non-fat dried milk. Then, membranes were incubated with primary antibodies overnight at 4 °C. The following primary antibodies were used: Bax (1:1000; Cell Signaling Technology, Danvers, MA, USA) and Bcl-2 (1:1000; Cell Signaling Technology, Danvers, MA, USA). The membranes were incubated with secondary antibodies and horseradish peroxidase (HRP)-conjugated anti-rabbit IgG (1:2000; Santa Cruz Biotechnology, Inc., Dallas, TX, USA) for 1 h at room temperature. To evaluate that blots were loaded with equal amounts of protein lysates, they were also incubated with an antibody for GAPDH HRP Conjugated (1:1000; Cell Signaling Technology). The relative expression of protein bands was visualized using an enhanced chemiluminescence system (Luminata Western HRP Substrates, Millipore Corporation, Billerica, MA, USA), and protein bands were obtained and quantified with a ChemiDoc™ MP System (Bio-Rad Laboratories S.r.l., Hercules, CA, USA) and analyzed with the software Image J 1.54d. The uncropped blots for Bax and Bcl-2 and relatives of GAPDH are available in the supplementary Figures S2 and S3, respectively.

4.8. Statistical Analysis

Statistical analysis of cell viability and Western blot was carried out using GraphPad Prism version 9.0 software (GraphPad Software, La Jolla, CA, USA). Multiple comparisons were performed using a one-way ANOVA test and the Bonferroni post hoc test. A p-value less than or equal to 0.05 was considered statistically significant. The results are expressed by the mean ± standard deviation (SD).

5. Conclusions

Δ^8-THC reduced A$\beta_{1\text{-}42}$-induced toxicity as a result of a reduction in ER stress. Indeed, Δ^8-THC restored proteostasis, increasing the expression of proteasome and ubiquitin subunits and reducing UPR, suggesting that misfolded/unfolded proteins were not accumulated but could be eliminated through the proteasome. As a consequence of the reduced ER stress, Δ^8-THC increased neuronal cell viability. The results suggested that Δ^8-THC may represent a novel neuroprotective agent in AD but also in other neurodegenerative diseases characterized by the accumulation of misfolded proteins.

Supplementary Materials: The following supporting information can be downloaded at: https://www.mdpi.com/article/10.3390/ijms24076598/s1.

Author Contributions: Conceptualization, E.M.; methodology, A.G.; software, L.C.; formal analysis, L.C.; investigation, A.G. and S.B.; resources, S.S., D.C. and F.P.; data curation, L.C.; writing—original draft preparation, A.G.; writing—review and editing, E.M.; supervision, E.M. All authors have read and agreed to the published version of the manuscript.

Funding: This study was supported by the current research fund 2023, Ministry of Health, Italy.

Institutional Review Board Statement: Not applicable.

Informed Consent Statement: Not applicable.

Data Availability Statement: The data presented in this study are openly available in the NCBI Sequence Read Archive at BioProject accession numbers PRJNA934843.

Acknowledgments: We want to sincerely thank Maria Sofia Basile for her assistance in the writing process.

Conflicts of Interest: The authors declare no conflict of interest. The funders had no role in the design of the study; in the collection, analyses, or interpretation of data; in the writing of the manuscript; or in the decision to publish the results.

References

1. Leng, F.; Edison, P. Neuroinflammation and microglial activation in Alzheimer disease: Where do we go from here? *Nat. Rev. Neurol.* **2021**, *17*, 157–172. [CrossRef] [PubMed]
2. Durairajan, S.S.K.; Selvarasu, K.; Bera, M.R.; Rajaram, K.; Iyaswamy, A.; Li, M. Alzheimer's Disease and other Tauopathies: Exploring Efficacy of Medicinal Plant-derived Compounds in Alleviating Tau-mediated Neurodegeneration. *Curr. Mol. Pharmacol.* **2022**, *15*, 361–379. [CrossRef]
3. Basile, M.S.; Bramanti, P.; Mazzon, E. Inosine in Neurodegenerative Diseases: From the Bench to the Bedside. *Molecules* **2022**, *27*, 4644. [CrossRef] [PubMed]
4. Kumar, A.; Sidhu, J.; Goyal, A.; Tsao, J.W. Alzheimer Disease. In *StatPearls*; StatPearls Publishing: Treasure Island, FL, USA, 2022.
5. Petit, D.; Fernandez, S.G.; Zoltowska, K.M.; Enzlein, T.; Ryan, N.S.; O'Connor, A.; Szaruga, M.; Hill, E.; Vandenberghe, R.; Fox, N.C.; et al. Aβ profiles generated by Alzheimer's disease causing PSEN1 variants determine the pathogenicity of the mutation and predict age at disease onset. *Mol. Psychiatry* **2022**, *27*, 2821–2832. [CrossRef]
6. Belaidi, A.A.; Masaldan, S.; Southon, A.; Kalinowski, P.; Acevedo, K.; Appukuttan, A.T.; Portbury, S.; Lei, P.; Agarwal, P.; Leurgans, S.E.; et al. Apolipoprotein E potently inhibits ferroptosis by blocking ferritinophagy. *Mol. Psychiatry* **2022**. [CrossRef] [PubMed]
7. Shi, M.; Chu, F.; Zhu, F.; Zhu, J. Impact of Anti-amyloid-β Monoclonal Antibodies on the Pathology and Clinical Profile of Alzheimer's Disease: A Focus on Aducanumab and Lecanemab. *Front. Aging Neurosci.* **2022**, *14*, 870517. [CrossRef]
8. Knopman, D.S.; Amieva, H.; Petersen, R.C.; Chetelat, G.; Holtzman, D.M.; Hyman, B.T.; Nixon, R.A.; Jones, D.T. Alzheimer disease. *Nat. Rev. Dis. Prim.* **2021**, *7*, 33. [CrossRef]
9. Cezar Prado, P.; Alencar Lima, J.; Hamerski, L.; Nascimento Renno, M. Natural Products with BACE1 and GSK3β Inhibitory Activity. *Mini Rev. Med. Chem.* **2022**. [CrossRef]
10. Chang, C.H.; Lin, C.H.; Lane, H.Y. Machine Learning and Novel Biomarkers for the Diagnosis of Alzheimer's Disease. *Int. J. Mol. Sci.* **2021**, *22*, 2761. [CrossRef]
11. Yu, H.; Wu, J. Amyloid-β: A double agent in Alzheimer's disease? *Biomed. Pharmacother.* **2021**, *139*, 111575. [CrossRef]
12. Goswami, P.; Afjal, M.A.; Akhter, J.; Mangla, A.; Khan, J.; Parvez, S.; Raisuddin, S. Involvement of endoplasmic reticulum stress in amyloid $\beta_{(1\text{-}42)}$-induced Alzheimer's like neuropathological process in rat brain. *Brain Res. Bull.* **2020**, *165*, 108–117. [CrossRef] [PubMed]
13. Ghemrawi, R.; Khair, M. Endoplasmic Reticulum Stress and Unfolded Protein Response in Neurodegenerative Diseases. *Int. J. Mol. Sci.* **2020**, *21*, 6127. [CrossRef] [PubMed]
14. Pardo-Moreno, T.; Gonzalez-Acedo, A.; Rivas-Dominguez, A.; Garcia-Morales, V.; Garcia-Cozar, F.J.; Ramos-Rodriguez, J.J.; Melguizo-Rodriguez, L. Therapeutic Approach to Alzheimer's Disease: Current Treatments and New Perspectives. *Pharmaceutics* **2022**, *14*, 1117. [CrossRef] [PubMed]
15. Reardon, S. FDA approves Alzheimer's drug lecanemab amid safety concerns. *Nature* **2023**, *613*, 227–228. [CrossRef]
16. Yeo-Teh, N.S.L.; Tang, B.L. A Review of Scientific Ethics Issues Associated with the Recently Approved Drugs for Alzheimer's Disease. *Sci. Eng. Ethics* **2023**, *29*, 2. [CrossRef] [PubMed]
17. Soderberg, L.; Johannesson, M.; Nygren, P.; Laudon, H.; Eriksson, F.; Osswald, G.; Moller, C.; Lannfelt, L. Lecanemab, Aducanumab, and Gantenerumab—Binding Profiles to Different Forms of Amyloid-Beta Might Explain Efficacy and Side Effects in Clinical Trials for Alzheimer's Disease. *Neurotherapeutics* **2022**. [CrossRef]
18. Dou, K.X.; Tan, M.S.; Tan, C.C.; Cao, X.P.; Hou, X.H.; Guo, Q.H.; Tan, L.; Mok, V.; Yu, J.T. Comparative safety and effectiveness of cholinesterase inhibitors and memantine for Alzheimer's disease: A network meta-analysis of 41 randomized controlled trials. *Alzheimer's Res. Ther.* **2018**, *10*, 126. [CrossRef]
19. Uddin, M.S.; Mamun, A.A.; Sumsuzzman, D.M.; Ashraf, G.M.; Perveen, A.; Bungau, S.G.; Mousa, S.A.; El-Seedi, H.R.; Bin-Jumah, M.N.; Abdel-Daim, M.M. Emerging Promise of Cannabinoids for the Management of Pain and Associated Neuropathological Alterations in Alzheimer's Disease. *Front. Pharmacol.* **2020**, *11*, 1097. [CrossRef]
20. Abate, G.; Uberti, D.; Tambaro, S. Potential and Limits of Cannabinoids in Alzheimer's Disease Therapy. *Biology* **2021**, *10*, 542. [CrossRef]
21. Leas, E.C. The Hemp Loophole: A Need to Clarify the Legality of Delta-8-THC and Other Hemp-Derived Tetrahydrocannabinol Compounds. *Am. J. Public Health* **2021**, *111*, 1927–1931. [CrossRef]
22. Tagen, M.; Klumpers, L.E. Review of delta-8-tetrahydrocannabinol (Delta(8) -THC): Comparative pharmacology with Delta(9)-THC. *Br. J. Pharmacol.* **2022**, *179*, 3915–3933. [CrossRef] [PubMed]
23. LoParco, C.R.; Rossheim, M.E.; Walters, S.T.; Zhou, Z.; Olsson, S.; Sussman, S.Y. Delta-8 tetrahydrocannabinol: A scoping review and commentary. *Addiction* **2023**. *Early View*. [CrossRef] [PubMed]

24. Puopolo, T.; Liu, C.; Ma, H.; Seeram, N.P. Inhibitory Effects of Cannabinoids on Acetylcholinesterase and Butyrylcholinesterase Enzyme Activities. *Med. Cannabis Cannabinoids* **2022**, *5*, 85–94. [CrossRef] [PubMed]
25. Giacobini, E.; Cuello, A.C.; Fisher, A. Reimagining cholinergic therapy for Alzheimer's disease. *Brain* **2022**, *145*, 2250–2275. [CrossRef]
26. Brodaty, H.; Breteler, M.M.; Dekosky, S.T.; Dorenlot, P.; Fratiglioni, L.; Hock, C.; Kenigsberg, P.A.; Scheltens, P.; De Strooper, B. The world of dementia beyond 2020. *J. Am. Geriatr. Soc.* **2011**, *59*, 923–927. [CrossRef]
27. Kruger, J.S.; Kruger, D.J. Delta-8-THC: Delta-9-THC's nicer younger sibling? *J. Cannabis Res.* **2022**, *4*, 4. [CrossRef]
28. Cao, C.; Li, Y.; Liu, H.; Bai, G.; Mayl, J.; Lin, X.; Sutherland, K.; Nabar, N.; Cai, J. The potential therapeutic effects of THC on Alzheimer's disease. *J. Alzheimer's Dis.* **2014**, *42*, 973–984. [CrossRef]
29. Nitzan, K.; Ellenbogen, L.; Bentulila, Z.; David, D.; Franko, M.; Break, E.P.; Zoharetz, M.; Shamir, A.; Sarne, Y.; Doron, R. An Ultra-Low Dose of Δ9-Tetrahydrocannabinol Alleviates Alzheimer's Disease-Related Cognitive Impairments and Modulates TrkB Receptor Expression in a 5XFAD Mouse Model. *Int. J. Mol. Sci.* **2022**, *23*, 9449. [CrossRef]
30. Chen, R.; Zhang, J.; Fan, N.; Teng, Z.Q.; Wu, Y.; Yang, H.; Tang, Y.P.; Sun, H.; Song, Y.; Chen, C. Delta9-THC-caused synaptic and memory impairments are mediated through COX-2 signaling. *Cell* **2013**, *155*, 1154–1165. [CrossRef]
31. Wang, Y.H.; Hong, Y.Z.; Yan, J.Y.; Brown, B.; Lin, X.Y.; Zhang, X.L.; Shen, N.; Li, M.H.; Cai, J.F.; Gordon, M.; et al. Low-Dose Delta-9-Tetrahydrocannabinol as Beneficial Treatment for Aged APP/PS1 Mice. *Int. J. Mol. Sci.* **2022**, *23*, 2757. [CrossRef]
32. Haghani, M.; Shabani, M.; Javan, M.; Motamedi, F.; Janahmadi, M. CB1 cannabinoid receptor activation rescues amyloid β-induced alterations in behaviour and intrinsic electrophysiological properties of rat hippocampal CA1 pyramidal neurones. *Cell. Physiol. Biochem.* **2012**, *29*, 391–406. [CrossRef] [PubMed]
33. Aso, E.; Palomer, E.; Juves, S.; Maldonado, R.; Munoz, F.J.; Ferrer, I. CB1 agonist ACEA protects neurons and reduces the cognitive impairment of AβPP/PS1 mice. *J. Alzheimer's Dis.* **2012**, *30*, 439–459. [CrossRef] [PubMed]
34. Magham, S.V.; Thaggikuppe Krishnamurthy, P.; Shaji, N.; Mani, L.; Balasubramanian, S. Cannabinoid receptor 2 selective agonists and Alzheimer's disease: An insight into the therapeutic potentials. *J. Neurosci. Res.* **2021**, *99*, 2888–2905. [CrossRef]
35. Soto-Mercado, V.; Mendivil-Perez, M.; Jimenez-Del-Rio, M.; Velez-Pardo, C. Multi-Target Effects of the Cannabinoid CP55940 on Familial Alzheimer's Disease PSEN1 E280A Cholinergic-Like Neurons: Role of CB1 Receptor. *J. Alzheimer's Dis.* **2021**, *82*, S359–S378. [CrossRef] [PubMed]
36. Singh, R.; Kaur, N.; Dhingra, N.; Kaur, T. Protein misfolding, ER stress and chaperones: An approach to develop chaperone-based therapeutics for Alzheimer's disease. *Int. J. Neurosci.* **2022**, 1–21. [CrossRef]
37. Penke, B.; Bogar, F.; Crul, T.; Santha, M.; Toth, M.E.; Vigh, L. Heat Shock Proteins and Autophagy Pathways in Neuroprotection: From Molecular Bases to Pharmacological Interventions. *Int. J. Mol. Sci.* **2018**, *19*, 325. [CrossRef]
38. Eletto, D.; Dersh, D.; Argon, Y. GRP94 in ER quality control and stress responses. *Semin. Cell Dev. Biol.* **2010**, *21*, 479–485. [CrossRef]
39. Hoozemans, J.J.; van Haastert, E.S.; Nijholt, D.A.; Rozemuller, A.J.; Eikelenboom, P.; Scheper, W. The unfolded protein response is activated in pretangle neurons in Alzheimer's disease hippocampus. *Am. J. Pathol.* **2009**, *174*, 1241–1251. [CrossRef] [PubMed]
40. Ohno, M. PERK as a hub of multiple pathogenic pathways leading to memory deficits and neurodegeneration in Alzheimer's disease. *Brain Res. Bull.* **2018**, *141*, 72–78. [CrossRef]
41. Duran-Aniotz, C.; Cornejo, V.H.; Espinoza, S.; Ardiles, A.O.; Medinas, D.B.; Salazar, C.; Foley, A.; Gajardo, I.; Thielen, P.; Iwawaki, T.; et al. IRE1 signaling exacerbates Alzheimer's disease pathogenesis. *Acta Neuropathol.* **2017**, *134*, 489–506. [CrossRef]
42. Li, J.Q.; Yu, J.T.; Jiang, T.; Tan, L. Endoplasmic reticulum dysfunction in Alzheimer's disease. *Mol. Neurobiol.* **2015**, *51*, 383–395. [CrossRef] [PubMed]
43. Fonseca, S.G.; Ishigaki, S.; Oslowski, C.M.; Lu, S.; Lipson, K.L.; Ghosh, R.; Hayashi, E.; Ishihara, H.; Oka, Y.; Permutt, M.A.; et al. Wolfram syndrome 1 gene negatively regulates ER stress signaling in rodent and human cells. *J. Clin. Investig.* **2010**, *120*, 744–755. [CrossRef] [PubMed]
44. Chen, S.; Acosta, D.; Fu, H. New unexpected role for Wolfram Syndrome protein WFS1: A novel therapeutic target for Alzheimer's disease? *Neural Regen. Res.* **2023**, *18*, 1501–1502. [CrossRef] [PubMed]
45. Chen, S.; Acosta, D.; Li, L.; Liang, J.; Chang, Y.; Wang, C.; Fitzgerald, J.; Morrison, C.; Goulbourne, C.N.; Nakano, Y.; et al. Wolframin is a novel regulator of tau pathology and neurodegeneration. *Acta Neuropathol.* **2022**, *143*, 547–569. [CrossRef]
46. Olzmann, J.A.; Kopito, R.R.; Christianson, J.C. The mammalian endoplasmic reticulum-associated degradation system. *Cold Spring Harb. Perspect. Biol.* **2013**, *5*, a013185. [CrossRef]
47. Zhu, B.; Jiang, L.; Huang, T.; Zhao, Y.; Liu, T.; Zhong, Y.; Li, X.; Campos, A.; Pomeroy, K.; Masliah, E.; et al. ER-associated degradation regulates Alzheimer's amyloid pathology and memory function by modulating gamma-secretase activity. *Nat. Commun.* **2017**, *8*, 1472. [CrossRef]
48. Montibeller, L.; de Belleroche, J. Amyotrophic lateral sclerosis (ALS) and Alzheimer's disease (AD) are characterised by differential activation of ER stress pathways: Focus on UPR target genes. *Cell Stress Chaperones* **2018**, *23*, 897–912. [CrossRef]
49. Abisambra, J.F.; Jinwal, U.K.; Blair, L.J.; O'Leary, J.C., 3rd; Li, Q.; Brady, S.; Wang, L.; Guidi, C.E.; Zhang, B.; Nordhues, B.A.; et al. Tau accumulation activates the unfolded protein response by impairing endoplasmic reticulum-associated degradation. *J. Neurosci.* **2013**, *33*, 9498–9507. [CrossRef]
50. Meier, S.; Bell, M.; Lyons, D.N.; Ingram, A.; Chen, J.; Gensel, J.C.; Zhu, H.; Nelson, P.T.; Abisambra, J.F. Identification of Novel Tau Interactions with Endoplasmic Reticulum Proteins in Alzheimer's Disease Brain. *J. Alzheimer's Dis.* **2015**, *48*, 687–702. [CrossRef]

51. Avezov, E.; Frenkel, Z.; Ehrlich, M.; Herscovics, A.; Lederkremer, G.Z. Endoplasmic reticulum (ER) mannosidase I is compartmentalized and required for N-glycan trimming to Man5-6GlcNAc2 in glycoprotein ER-associated degradation. *Mol. Biol. Cell* **2008**, *19*, 216–225. [CrossRef]
52. Olivari, S.; Molinari, M. Glycoprotein folding and the role of EDEM1, EDEM2 and EDEM3 in degradation of folding-defective glycoproteins. *FEBS Lett.* **2007**, *581*, 3658–3664. [CrossRef] [PubMed]
53. Alcock, F.; Swanton, E. Mammalian OS-9 is upregulated in response to endoplasmic reticulum stress and facilitates ubiquitination of misfolded glycoproteins. *J. Mol. Biol.* **2009**, *385*, 1032–1042. [CrossRef] [PubMed]
54. van der Goot, A.T.; Pearce, M.M.P.; Leto, D.E.; Shaler, T.A.; Kopito, R.R. Redundant and Antagonistic Roles of XTP3B and OS9 in Decoding Glycan and Non-glycan Degrons in ER-Associated Degradation. *Mol. Cell* **2018**, *70*, 516–530.e6. [CrossRef]
55. Nowakowska-Golacka, J.; Czapiewska, J.; Sominka, H.; Sowa-Rogozinska, N.; Slominska-Wojewodzka, M. EDEM1 Regulates Amyloid Precursor Protein (APP) Metabolism and Amyloid-β Production. *Int. J. Mol. Sci.* **2021**, *23*, 117. [CrossRef]
56. Quistgaard, E.M. BAP31: Physiological functions and roles in disease. *Biochimie* **2021**, *186*, 105–129. [CrossRef]
57. Wang, T.; Chen, J.; Hou, Y.; Yu, Y.; Wang, B. BAP31 deficiency contributes to the formation of amyloid-β plaques in Alzheimer's disease by reducing the stability of RTN3. *FASEB J.* **2019**, *33*, 4936–4946. [CrossRef]
58. Kobayashi, T.; Manno, A.; Kakizuka, A. Involvement of valosin-containing protein (VCP)/p97 in the formation and clearance of abnormal protein aggregates. *Genes Cells* **2007**, *12*, 889–901. [CrossRef]
59. Chen, B.; Mariano, J.; Tsai, Y.C.; Chan, A.H.; Cohen, M.; Weissman, A.M. The activity of a human endoplasmic reticulum-associated degradation E3, gp78, requires its Cue domain, RING finger, and an E2-binding site. *Proc. Natl. Acad. Sci. USA* **2006**, *103*, 341–346. [CrossRef] [PubMed]
60. Chen, X.; Duan, L.H.; Luo, P.C.; Hu, G.; Yu, X.; Liu, J.; Lu, H.; Liu, B. FBXO6-Mediated Ubiquitination and Degradation of Ero1L Inhibits Endoplasmic Reticulum Stress-Induced Apoptosis. *Cell. Physiol. Biochem.* **2016**, *39*, 2501–2508. [CrossRef]
61. Russo, A. Understanding the mammalian TRAP complex function(s). *Open Biol.* **2020**, *10*, 190244. [CrossRef] [PubMed]
62. Elia, F.; Yadhanapudi, L.; Tretter, T.; Romisch, K. The N-terminus of Sec61p plays key roles in ER protein import and ERAD. *PLoS ONE* **2019**, *14*, e0215950. [CrossRef] [PubMed]
63. Romisch, K. A Case for Sec61 Channel Involvement in ERAD. *Trends Biochem. Sci.* **2017**, *42*, 171–179. [CrossRef] [PubMed]
64. Sai, X.; Kawamura, Y.; Kokame, K.; Yamaguchi, H.; Shiraishi, H.; Suzuki, R.; Suzuki, T.; Kawaichi, M.; Miyata, T.; Kitamura, T.; et al. Endoplasmic reticulum stress-inducible protein, Herp, enhances presenilin-mediated generation of amyloid β-protein. *J. Biol. Chem.* **2002**, *277*, 12915–12920. [CrossRef]
65. Ye, Y.; Shibata, Y.; Yun, C.; Ron, D.; Rapoport, T.A. A membrane protein complex mediates retro-translocation from the ER lumen into the cytosol. *Nature* **2004**, *429*, 841–847. [CrossRef] [PubMed]
66. Lilley, B.N.; Ploegh, H.L. A membrane protein required for dislocation of misfolded proteins from the ER. *Nature* **2004**, *429*, 834–840. [CrossRef] [PubMed]
67. Liu, Y.; Ye, Y. Roles of p97-associated deubiquitinases in protein quality control at the endoplasmic reticulum. *Curr. Protein Pept. Sci.* **2012**, *13*, 436–446. [CrossRef] [PubMed]
68. Kumar Deshmukh, F.; Yaffe, D.; Olshina, M.A.; Ben-Nissan, G.; Sharon, M. The Contribution of the 20S Proteasome to Proteostasis. *Biomolecules* **2019**, *9*, 190. [CrossRef]
69. Zhao, X.; Yang, J. Amyloid-β peptide is a substrate of the human 20S proteasome. *ACS Chem. Neurosci.* **2010**, *1*, 655–660. [CrossRef]
70. Cozachenco, D.; Ribeiro, F.C.; Ferreira, S.T. Defective proteostasis in Alzheimer's disease. *Ageing Res. Rev.* **2023**, *85*, 101862. [CrossRef]
71. Wu, Y.; Deng, Y.; Zhang, S.; Luo, Y.; Cai, F.; Zhang, Z.; Zhou, W.; Li, T.; Song, W. Amyloid-β precursor protein facilitates the regulator of calcineurin 1-mediated apoptosis by downregulating proteasome subunit α type-5 and proteasome subunit β type-7. *Neurobiol. Aging* **2015**, *36*, 169–177. [CrossRef]
72. Park, H.M.; Kim, J.A.; Kwak, M.K. Protection against amyloid beta cytotoxicity by sulforaphane: Role of the proteasome. *Arch. Pharmacal Res.* **2009**, *32*, 109–115. [CrossRef]
73. Gaoni, Y.; Mechoulam, R. The isolation and structure of delta-1-tetrahydrocannabinol and other neutral cannabinoids from hashish. *J. Am. Chem. Soc.* **1971**, *93*, 217–224. [CrossRef] [PubMed]
74. Yang, S.G.; Wang, W.Y.; Ling, T.J.; Feng, Y.; Du, X.T.; Zhang, X.; Sun, X.X.; Zhao, M.; Xue, D.; Yang, Y.; et al. alpha-Tocopherol quinone inhibits beta-amyloid aggregation and cytotoxicity, disaggregates preformed fibrils and decreases the production of reactive oxygen species, NO and inflammatory cytokines. *Neurochem. Int.* **2010**, *57*, 914–922. [CrossRef] [PubMed]
75. Gugliandolo, A.; Chiricosta, L.; Silvestro, S.; Bramanti, P.; Mazzon, E. α-Tocopherol Modulates Non-Amyloidogenic Pathway and Autophagy in an In Vitro Model of Alzheimer's Disease: A Transcriptional Study. *Brain Sci.* **2019**, *9*, 196. [CrossRef] [PubMed]
76. Silvestro, S.; Chiricosta, L.; Gugliandolo, A.; Iori, R.; Rollin, P.; Perenzoni, D.; Mattivi, F.; Bramanti, P.; Mazzon, E. The Moringin/α-CD Pretreatment Induces Neuroprotection in an In Vitro Model of Alzheimer's Disease: A Transcriptomic Study. *Curr. Issues Mol. Biol.* **2021**, *43*, 197–214. [CrossRef] [PubMed]
77. Castillo, W.O.; Aristizabal-Pachon, A.F.; de Lima Montaldi, A.P.; Sakamoto-Hojo, E.T.; Takahashi, C.S. Galanthamine decreases genotoxicity and cell death induced by β-amyloid peptide in SH-SY5Y cell line. *Neurotoxicology* **2016**, *57*, 291–297. [CrossRef]

78. Castillo, W.O.; Aristizabal-Pachon, A.F.; Sakamoto-Hojo, E.; Gasca, C.A.; Cabezas-Fajardo, F.A.; Takahashi, C. *Caliphruria subedentata* (Amaryllidaceae) decreases genotoxicity and cell death induced by β-amyloid peptide in SH-SY5Y cell line. *Mutat. Res./Genet. Toxicol. Environ. Mutagen.* **2018**, *836*, 54–61. [CrossRef]
79. Mei, Z.; Yan, P.; Situ, B.; Mou, Y.; Liu, P. Cryptotanshinione inhibits β-amyloid aggregation and protects damage from β-amyloid in SH-SY5Y cells. *Neurochem. Res.* **2012**, *37*, 622–628. [CrossRef]
80. Seino, S.; Kimoto, T.; Yoshida, H.; Tanji, K.; Matsumiya, T.; Hayakari, R.; Seya, K.; Kawaguchi, S.; Tsuruga, K.; Tanaka, H.; et al. Gnetin C, a resveratrol dimer, reduces amyloid-β 1-42 (Aβ42) production and ameliorates Aβ42-lowered cell viability in cultured SH-SY5Y human neuroblastoma cells. *Biomed. Res.* **2018**, *39*, 105–115. [CrossRef]
81. Cai, Y.; Xiao, R.; Zhang, Y.; Xu, D.; Wang, N.; Han, M.; Zhang, Y.; Zhang, L.; Zhou, W. DHPA Protects SH-SY5Y Cells from Oxidative Stress-Induced Apoptosis via Mitochondria Apoptosis and the Keap1/Nrf2/HO-1 Signaling Pathway. *Antioxidants* **2022**, *11*, 1794. [CrossRef]
82. Zhang, W.; Yang, Y.; Xiang, Z.; Cheng, J.; Yu, Z.; Wang, W.; Hu, L.; Ma, F.; Deng, Y.; Jin, Z.; et al. MRTF-A-mediated protection against amyloid-β-induced neuronal injury correlates with restoring autophagy via miR-1273g-3p/mTOR axis in Alzheimer models. *Aging* **2022**, *14*, 4305–4325. [CrossRef] [PubMed]
83. Bhanukiran, K.; Gajendra, T.A.; Krishnamurthy, S.; Singh, S.K.; Hemalatha, S. Discovery of multi-target directed 3-OH pyrrolidine derivatives through a semisynthetic approach from alkaloid vasicine for the treatment of Alzheimer's disease. *Eur. J. Med. Chem.* **2023**, *249*, 115145. [CrossRef] [PubMed]
84. Song, Z.; He, C.; Yu, W.; Yang, M.; Li, Z.; Li, P.; Zhu, X.; Xiao, C.; Cheng, S. Baicalin Attenuated $A\beta_{1\text{-}42}$-Induced Apoptosis in SH-SY5Y Cells by Inhibiting the Ras-ERK Signaling Pathway. *BioMed Res. Int.* **2022**, *2022*, 9491755. [CrossRef]
85. Bolger, A.M.; Lohse, M.; Usadel, B. Trimmomatic: A flexible trimmer for Illumina sequence data. *Bioinformatics* **2014**, *30*, 2114–2120. [CrossRef] [PubMed]
86. Dobin, A.; Davis, C.A.; Schlesinger, F.; Drenkow, J.; Zaleski, C.; Jha, S.; Batut, P.; Chaisson, M.; Gingeras, T.R. STAR: Ultrafast universal RNA-seq aligner. *Bioinformatics* **2013**, *29*, 15–21. [CrossRef]
87. Anders, S.; Pyl, P.T.; Huber, W. HTSeq—A Python framework to work with high-throughput sequencing data. *Bioinformatics* **2015**, *31*, 166–169. [CrossRef]
88. Love, M.I.; Huber, W.; Anders, S. Moderated estimation of fold change and dispersion for RNA-seq data with DESeq2. *Genome Biol.* **2014**, *15*, 550. [CrossRef]
89. Durinck, S.; Moreau, Y.; Kasprzyk, A.; Davis, S.; De Moor, B.; Brazma, A.; Huber, W. BioMart and Bioconductor: A powerful link between biological databases and microarray data analysis. *Bioinformatics* **2005**, *21*, 3439–3440. [CrossRef]

Disclaimer/Publisher's Note: The statements, opinions and data contained in all publications are solely those of the individual author(s) and contributor(s) and not of MDPI and/or the editor(s). MDPI and/or the editor(s) disclaim responsibility for any injury to people or property resulting from any ideas, methods, instructions or products referred to in the content.